2009 American Control Conference
Hyatt Regency Riverfront, St. Louis, MO, USA
June 10-12, 2009

Air Flow Control in Fuel Cell Systems: An Extremum Seeking Approach

Yiyao A. Chang and Scott J. Moura

Abstract—**This paper examines the problem of maximizing net power output in a polymer electrolyte membrane (PEM) fuel cell system. The net power production depends heavily on the oxygen excess ratio in the cathode. However, the time-varying parameters and complex nonlinear dynamics of the system present many challenges to regulating oxygen excess ratio under all operating conditions. A constrained extremum seeking control architecture is presented to effectively regulate oxygen excess ratio about an optimum value that maximizes net power output over a broad range of operating conditions. Simulation results demonstrate that this control technique improves fuel cell system performance and our constrained optimization approach enables faster convergence rates for an admissible level of overshoot.**

I. Introduction

THIS paper investigates an air flow control strategy for optimizing the net power output of fuel cell systems, subject to time-varying parameters. The extremum seeking control approach ensures the fuel cell system operates at peak performance under all operating conditions. Moreover, the proposed algorithm avoids excessive power waste and oxygen starvation [1] by imposing constraints on the air supply subsystem. This is particularly important for increasing the robustness of fuel cell systems, which is generally difficult to achieve due to the challenge of accurately modeling the highly coupled electrochemical, thermodynamic, heat transfer, material, and fluid dynamics. In this paper, we consider polymer electrolyte membrane (PEM) fuel cells, which are popular in automotive applications due to their low operating temperature. However, our extremum seeking approach is extendible to a general class of nonlinear dynamic systems, including fuel cell systems with alternative electrolytes.

The fuel cell control engineering literature is rich with both adaptive and optimal control techniques for power management. Pukrushpan *et al.* developed a nonlinear state-space model and used linear-quadratic-Gaussian (LQG) techniques to control the air supply subsystem [2]. This work introduced a physics-based fuel cell system model, but the control design does not explicitly maximize power output over the entire operating range, as suggested by [3]. To achieve this goal, Yang *et al.* [4] reduced a model of two inputs (hydrogen and air flow rates) and two outputs (cell voltage and current) to a single-input single-output (SISO) system to regulate fuel cell output voltage by adjusting air flow rate using model identification adaptive control (MIAC). While both simulation and experimental data demonstrate that adaptive control can be implemented to adjust for changes in system parameters effectively, over-simplified models can sometimes produce erroneous calculations and inefficient performance characteristics. Golbert *et al.* developed a high fidelity, spatial-time dependent model and applied model predictive control (MPC) to satisfy a set of desired power requirements [5]. Although nonlinear multivariable MPC generally ensures accurate control under external disturbances, on-line optimization can be computationally intensive, particularly for the complicated fuel cell system models used in the literature [2], [5]. Ideally, it is more desirable to maximize fuel cell performance via control algorithms that are both computationally efficient and self-optimizing with respect to time-varying parameters and model uncertainty.

The above survey briefly examines several approaches for air flow control in fuel cell systems. These methods generally regulate the air supply to the cathode at a fixed level, either via adaptive or optimal control techniques. However, the optimal air supply may vary as system parameters, such as stack temperature and membrane humidity, drift away from their nominal values. Hence, we investigate the impact of oxygen supply, stack temperature, and membrane humidity on net power output, by analyzing the first principles model presented in [6] and [7]. This particular model assumes that the fuel stack water and temperature dynamics are controlled independently, although more recent work has included the dynamic coupling between air flow, membrane water content [8], and stack temperature [5]. In practice, this assumption will likely be violated, since water management represents one of the most challenging obstacles in fuel cell control and is currently an active area of research, e.g., [8], [9]. To mitigate the uncertainty imposed by water and temperature dynamics, we apply the method of extremum seeking (ES) control, a non-model based and self-optimizing algorithm, to seek for the optimal operating point using a gradient-based search. ES control is sensitive to water and temperature dynamics without requiring an explicit model for control, thus reconciling the tradeoff between computational efficiency and optimal performance.

A similar extremum seeking approach developed in [10] tracks the fuel cell stack's maximum power point by controlling the current input at the DC/DC power conversion electronics level, while providing constant oxygen supply. In

Manuscript received March 22, 2009. This work was supported in part by the Rackham Conference Travel Grant at the University of Michigan, Ann Arbor and the National Science Foundation Graduate Research Fellowship Program.

Y. A. Chang is with the Department of Applications Engineering, National Instruments, Austin, TX 78759 and S. J. Moura is with the Department of Mechanical Engineering, University of Michigan, Ann Arbor, MI 48109-2133 USA (e-mail: andy.chang@ni.com; sjmoura@umich.edu).

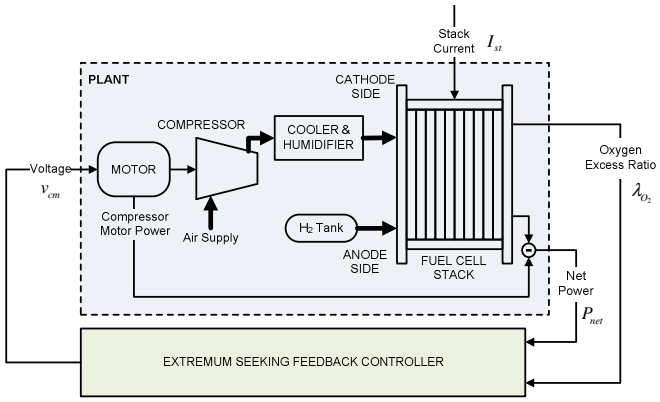

Fig. 1. Fuel cell system model, comprised of fuel cell stack, anode, cathode, cooler, humidifier, compressor, and compressor motor. Air flow in the fuel cell system is regulated using an extremum seeking controller.

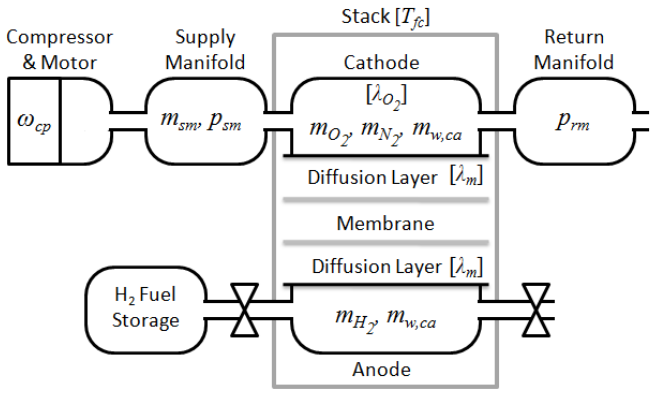

Fig. 2. Air supply subsystem, indicating model state variables, oxygen excess ratio λ_{O2}, stack temperature T_{fc}, and membrane water content λ_m.

contrast, this paper focuses on maximizing net fuel cell system power output at the air flow control level. By controlling the air flow supply to the cathode, the amount of reactant oxygen is managed to ensure proper balance of stack power output and compressor motor power draw. Moreover, managing the amount of reactant oxygen enables some controllability over preventing oxygen starvation and membrane dehydration. This paper thus adds two new contributions to research on air flow control in fuel cell systems. First, it explicitly maximizes net power output by regulating air flow, thereby improving system efficiency and potentially catalyzing the market penetration of fuel cell systems. Second, it introduces a self-optimizing control scheme that maximizes net power production over the entire temperature and membrane hydration range. The paper's simulation results demonstrate an improvement in the fuel cell system's net power production can be achieved across various operating conditions relative to several standard control techniques.

The paper is organized as follows: Section II presents a summary of the fuel cell system model. A steady-state analysis of the fuel cell system is presented in Section III. Section IV provides the mathematical control problem formulation and Section V presents the key results. The paper's main conclusions are provided in Section IV.

TABLE I
FUEL CELL SYSTEM MODEL SPECIFICATIONS

Fuel Cell Stack	Membrane Type	Proton Electrolyte
	Maximum Power	75 kW
	No. of Cells (n)	381
	Membrane Thickness (t_m)	0.01275 cm
	Cell Active Area	280 cm^2
Compressor	Manufacturer	Allied Signals
	Type	Centrifugal
	Maximum Power	12.5 kW
Operating Parameters	Nominal Temperature (T_{fc})	353 K
	Nominal Membrane Water Content (λ_m)	14 (100% hydrated)

II. FUEL CELL SYSTEM MODEL

This section describes the fuel cell system model developed in [6], [7] that we use for analyzing the impact of oxygen supply, stack temperature, and membrane water content on net power output. The model describes the manifold filling dynamics, reactant partial pressures, and compressor inertia. The fuel cell system under consideration comprises a fuel cell stack, a compressor, anode and cathode manifolds, an air cooler, and a humidifier shown in Fig. 1. The fuel cell model used contains nine state variables, whose governing equations can be grouped into the cathode manifold, anode manifold, and compressor. In the manifolds, the governing equations model the mass flow and partial pressures of the reactants and products using mass and energy conservation laws. In the compressor, the governing equations model the inertial dynamics of the compressor and motor. The air compressor motor voltage v_{cm} is the controlled input, fuel cell stack current I_{st} is modeled as a disturbance input, while the performance output variables are net fuel cell system power P_{net} and oxygen excess ratio λ_{O2}. For clarity and completeness, we review the model equations and associated phenomena here, but readers interested in the complete details should refer to [6], [7]. The model's key parameters and component sizes are provided in Table I.

A. State Equations

This section describes the state equations corresponding to the air supply subsystem shown in Fig. 2. In the cathode, supply manifold, and return manifold, mass conservation yields the dynamic equations for the masses of oxygen m_{O2}, nitrogen m_{N2}, water $m_{w,ca}$, and supply manifold air m_{sm} given in (1)-(4). The rate of change of supply and return manifold pressures, p_{sm} and p_{rm}, are governed by energy conservation in (5)-(6).

$$\frac{d}{dt}m_{O_2} = W_{O_{2,in}} - W_{O_{2,out}} - W_{O_{2,rct}} \quad (1)$$

$$\frac{d}{dt}m_{N_2} = W_{N_{2,in}} - W_{N_{2,out}} \quad (2)$$

$$\frac{d}{dt}m_{w,ca} = W_{v,ca,in} - W_{v,ca,out} - W_{v,gen} - W_{v,mbr} \quad (3)$$

$$\frac{d}{dt}m_{sm} = W_{cp} - W_{sm} \quad (4)$$

$$\frac{d}{dt}p_{sm} = \frac{\gamma R}{M_a^{atm} V_{sm}}\left(W_{cp}T_{cp} - W_{sm}T_{sm}\right) \quad (5)$$

$$\frac{d}{dt}p_{rm} = \frac{RT_{fc}}{M_a^{ca} V_{rm}}\left(W_{ca} - W_{rm}\right) \quad (6)$$

where *m, p, W, γ, R, M, V, T* denote mass, pressure, mass flow rate, ratio of specific heat capacities for air, universal gas constant, molar mass of atmospheric air, volume, and temperature, respectively. The subscripts denote the location of the variable, e.g., W_{sm} is the mass flow rate of air in the supply manifold and T_{cp} is the temperature of air in the compressor.

The state equations for the anode model the rate of change of mass for hydrogen m_{H2} and water $m_{w,an}$, via the mass conservation principal in (7)-(8). These molecules arise as products of the chemical reaction in the stack.

$$\frac{d}{dt}m_{H_2} = W_{H_{2,in}} - W_{H_2,rct} \quad (7)$$

$$\frac{d}{dt}m_{w,an} = W_{v,an,in} - W_{v,mbr} \quad (8)$$

Air is supplied to the cathode by a compressor, which is powered by a motor that consumes energy generated from the fuel cell stack. The mass flow rate of air produced by the compressor W_{cp} is related to p_{sm} in (5) and the compressor speed ω_{cp}, which is governed by the following inertial dynamics:

$$J_{cp}\frac{d}{dt}\omega_{cp} = K_{cm}\left(v_{cm} - k_v\omega_{cp}\right) - \tau_{cp} \quad (9)$$

where J_{cp}, v_{cm}, τ_{cp}, K_{cm}, k_v denote the compressor inertia, motor input voltage, compressor driving torque, and motor constants, respectively. The model states are accumulated in the state vector

$$x = \left[m_{O_2}, m_{N_2}, m_{w,ca}, m_{sm}, p_{sm}, p_{rm}, m_{H_2}, m_{w,an}, \omega_{cp}\right]^T \quad (10)$$

B. Output Equations

A critically important variable in our analysis is the *oxygen excess ratio*, which describes the excess oxygen supplied to the cathode as follows:

$$\lambda_{O_2} = \frac{W_{O_2,in}}{W_{O_2,rct}} \quad (11)$$

where $W_{O2,in}$ and $W_{O2,rct}$ are the mass flow rates of oxygen entering the cathode and consumed by the chemical reaction, respectively. A value of λ_{O2} = 1 indicates the amount of oxygen supplied to the cathode is equal to the amount required by the stoichiometric chemical reaction $2H_2 + O_2 \rightarrow 2H_2O$. $W_{O2,rct}$ is directly proportional to the current drawn from the fuel cell stack I_{st} according to

$$W_{O_2,rct} = M_{O_2}\frac{nI_{st}}{4F} \quad (12)$$

where M_{O2}, n, and F are the oxygen molar mass, number of cells in the stack, and Faraday number, respectively. As a result, if a constant amount of oxygen is supplied to the cathode, λ_{O2} will decrease as I_{st} increases, which corresponds to oxygen starvation.

Since stack power is the product of current and voltage, let us review the phenomena associated with stack voltage. The stack voltage is comprised of the open circuit voltage E and voltage losses. These losses are typically categorized as activation loss v_{act}, ohmic loss v_{ohm}, and concentration loss v_{conc}, thus furnishing the following equation

$$v_{st} = E - v_{act} - v_{ohm} - v_{conc} \quad (10)$$

where each term on the right-hand side of (10) is calculated from physical properties and parameters empirically derived from experimental data [7]. These terms are generally nonlinear functions of both fuel cell stack temperature T_{fc} and water membrane content λ_m.

The power produced by the fuel cell stack is given by the product of stack current I_{st} and stack voltage v_{st}. The compressor motor draws power generated from the fuel cell stack according to the product of current I_{cm} and voltage v_{cm}. As a result, the net power produced by the entire fuel cell system is

$$P_{net} = I_{st}v_{st} - I_{cm}v_{cm} \quad (18)$$

where v_{cm} serves as the control input from the extremum seeking feedback loop and I_{cm} is defined by the compressor motor model.

III. Steady-State Analysis

Equation (11) indicates that high oxygen excess ratio λ_{O2} corresponds to more oxygen supplied to the cathode, which improves the power generated by the stack P_{st}. However, if λ_{O2} is too large, then net power P_{net} decreases due to excessive power demanded by the air compressor, as shown by (18). As a result, there exists an optimal value for λ_{O2} that maximizes P_{net} by trading off stack power production and compressor motor power consumption.

Using the fuel cell system model developed in [7], we investigate the effect of varying system parameters on the optimal value of λ_{O2}. Fig. 3 demonstrates that the value of P_{net} increases as T_{fc} increases, since more energy is released by the

governing chemical reaction. Also, as the fuel cell membrane water content increases (zero hydration at λ_m=0; full hydration at λ_m=14), P_{net} also increases, since high membrane humidity promotes high proton conductivity. Moreover, the range of maximum net power points for varying stack temperatures changes depending on membrane water content. At lower membrane water content values (e.g. λ_m=4), the range of maximum net power values is more drastic compared to when the membrane is fully hydrated.

It is most interesting to note that the optimal value of λ_{O2} fluctuates and ranges between 2.4 and 2.7, which is different from the results found in [6], [7], [11], [12]. This implies that improved performance may be achieved by identifying the optimal λ_{O2} value and regulating the system about this point. Since the optimal value of λ_{O2} changes with respect to these time-varying parameters, an on-line optimization control scheme is necessary to achieve maximum power output over the entire operating range.

IV. Extremum Seeking Problem Formulation

A. Optimization Formulation

The goal of this paper is to maximize the net power output P_{net} of the fuel system by means of air flow control. This problem can be summarized mathematically as:

Maximize: $$P_{net} = J(x,u,w) \tag{19}$$

Subject to: $$\dot{x} = f(x,u,w) \tag{20}$$

$$x \in X \tag{21}$$

$$u \in U \tag{22}$$

where the objective $J(x,u,w)$ is the system output function from (18) relating the model states x in (10), control input u, and disturbance inputs w to the objective function value. In the fuel cell system model discussed in this paper, u corresponds to the compressor motor voltage v_{cm}, and the disturbance input w corresponds to the demanded fuel cell stack current I_{st}. The optimization is subject to the fuel cell system dynamics $f(x,u,w)$ briefly surveyed in Section II, and the set constraints X and U, representing a feasible sets of states and controls, respectively. We refer to these set constraints as admissible states and controls.

As discussed in Section III, the oxygen excess ratio λ_{O2} (functionally dependent on the states x) is a critical value for understanding how mass air flow relates to net power. Therefore, if we require the fuel cell system to operate within some neighborhood of the maximum net power point, it may be reasonable to impose simple bounds on λ_{O2} to avoid oxygen starvation and membrane dehydration. This is mathematically represented by the set constraint

$$X = \{x : \lambda_{O_2} \in [1.4, 3.0]\} \tag{23}$$

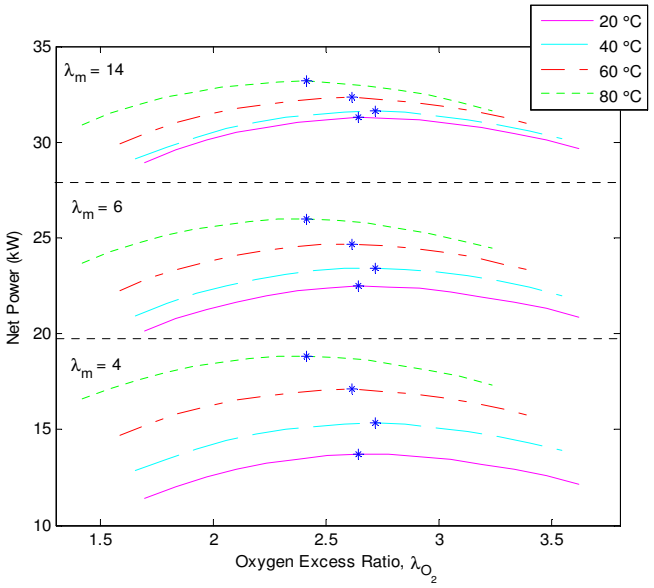

Fig. 3. Fuel cell system net power P_{net} vs. oxygen excess ratio λ_{O2} for stack current I_{st}=150A at different membrane water content λ_m values (λ_m = 0 and λ_m = 14 are 0% and 100% hydration, respectively).

Imposing this constraint within the control design requires a way to directly measure or accurately estimate λ_{O2}. For the present investigation, we assume such a method exists (e.g. using a Luenberger observer in [7]) and it does not significantly alter the model dynamics or output equations.

Actuator saturation constraints typically bound the set of admissible controls. In the case of a fuel cell system, this corresponds to minimum and maximum voltage inputs to the compressor motor. Hence, the set constraint U is defined as:

$$U = \{u : v_{cm} \in [0\text{V}, 220\text{V}]\} \tag{24}$$

The maximum compressor motor voltage corresponds directly to the compressor's maximum power capacity.

B. Extremum Seeking Control Architecture

To maximize net fuel cell system power, we employ a simple yet widely studied extremum seeking (ES) scheme [13]-[17] for static nonlinear maps, shown in Fig. 4, adapted to account for the inequality constraints given by (23) and (24). Before embarking on a detailed discussion of this method, we give an intuitive explanation of how the approach works, which can also be found in [13]-[15], but is presented here for completeness.

The control scheme applies a slow periodic perturbation $a\sin \omega t$ to the signal $\hat{u}$, which is the current estimate of the optimum value u^*. If the perturbation is slow enough, then the plant appears as a static nonlinear map $J(u)$ from the view of the extremum seeking loop. Hence, the plant outputs a periodic signal y. The band-pass filter then eliminates the DC component of y (or the augmented objective function value in the constrained case shown in Fig. 4. If the plant has a static maximum, as is the case for the fuel cell system in this study, then the output of the band-pass filter η will be in phase or out

of phase with the perturbation signal $a\sin \omega t$ if $\hat{u}$ is less than or greater than u^*, respectively. This property is important, because when the signal η is multiplied by the perturbation signal $\sin \omega t$, the resulting signal ξ has a DC component that is greater than or less than zero if $\hat{u}$ is less than or greater than u^*, respectively. Therefore, the signal ξ can be thought of as the sensitivity $(a^2/2)\, J'(\hat{u})$ and we may use a gradient update law $\dot{\hat{u}} = k(a^2/2)\, J'(\hat{u})$ to force $\hat{u}$ to converge to u^*.

This method for seeking extrema of static nonlinear maps requires the following assumptions about the closed loop system, which assist in selecting the ES parameters ω, a, k, and designing the band-pass filter:

Assumption 1: The ES perturbation frequency ω is selected to ensure significant time scale separation between the ES feedback loop and plant dynamics. Therefore, the plant dynamics in (20) appear as instantaneous, and the objective function in (19) reduces to $J(u)$. This assumption enables the use of a very simple ES control scheme for static maps. We note that other ES formulations exist without the time scale separation assumption, but they are generally much more complicated (e.g. [13], [14], [16], [18], [19]).

Assumption 2: The objective function is locally convex with respect to the control, and has a maximum value of $J(u^*)$.

Assumption 3: The values of k and a are sufficiently small to ensure the closed loop system remains stable for all time. In practice, however, one desires to set k and a as large as possible to increase convergence speed. As a result, the selection of these parameters involves a trade-off between convergence rate and stability. The proposed constrained extremum seeking approach eliminates this tradeoff to a certain degree, as discussed in Section V-B.

Assumption 4: As discussed in [14], the signals $a\sin \omega t$ and η must be

1. in phase for $\hat{u} < u^*$
2. out of phase for $\hat{u} > u^*$

for $\hat{u}$ to converge to u^*. This property must be satisfied by designing a band-pass filter which does not impose unwarranted phase lead as to violate the above assumption. Moreover, the band-pass filter must not attenuate the sinusoidal perturbation frequency, thus bounding the cutoff frequency from below.

Remark: Butterworth filters are particularly useful for designing a band-pass filter that satisfies the assumptions above, due to the following three properties: (1) The pass band contains the perturbation frequency and is maximally flat with unity magnitude. (2) The phase response can be tuned to zero at the perturbation frequency by appropriately selecting the cutoff frequencies. (3) Frequency components greater than

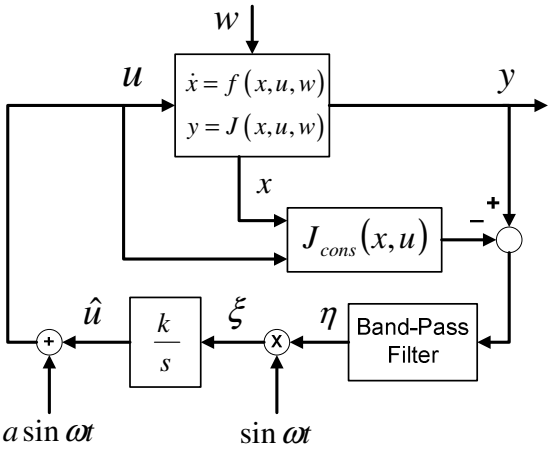

Fig. 4. Extremum seeking (ES) control scheme. The perturbation frequency ω is chosen to ensure large time scale separation between the plant and feedback loop. Hence, the plant appears as a static nonlinear map $J(u)$ from the viewpoint of ES. J_{cons} denotes the penalty function term.

the perturbation frequency are attenuated. This is important because when η is demodulated, the DC component of ξ accurately represents the phase shift between perturbation and output signals.

The inequality constraints are enforced by transforming (23) and (24) into exterior-point penalty functions, given by

$$J_{cons} = J_{cons,u} + J_{cons,x} \tag{27}$$

$$J_{cons,u} = \left[100 \times \max \left\{ \frac{v_{cm}^{\min} - v_{cm}}{v_{cm}^{\min}}, 0, \frac{v_{cm} - v_{cm}^{\max}}{v_{cm}^{\max}} \right\} \right]^2 \tag{28}$$

$$J_{cons,x} = \left[100 \times \max \left\{ \frac{\lambda_{O_2}^{\min} - \lambda_{O_2}}{\lambda_{O_2}^{\min}}, 0, \frac{\lambda_{O_2} - \lambda_{O_2}^{\max}}{\lambda_{O_2}^{\max}} \right\} \right]^2 \tag{29}$$

and augmenting these soft constraints to the objective function $J(u)$. Here, we apply quadratic penalty functions that penalize the square of the percentage excursion outside the desired operating range. The concept of penalty functions is fundamental to constrained optimization theory [20] and similar to existing extremum seeking techniques [21]. However, the application of constrained optimization techniques to the extremum seeking architecture studied in [14] is novel, to the authors' knowledge.

V. Simulation Results and Discussion

A. Control Architectures

To evaluate the performance characteristics of our proposed extremum seeking controller, we compare it to two simpler control architectures, referred to as static feedforward (sFF) and static feedforward with PI control (sFF + PI).

The idea behind the sFF control configuration is to use a direct measurement of the disturbance input I_{st} to compute the compressor motor voltage required to maintain the oxygen excess ratio $\lambda_{O2} = 2$. This takes the form of the open loop static feedforward compensator $g_{sFF}(I_{st}) = 0.67I_{st} + 33.55$ in Fig. 5(a), which is synthesized by inverting the DC gain of the plant. This controller is taken directly from [7] and is very simple to implement, but lacks the robustness properties of feedback controllers. Moreover, the oxygen excess ratio will not be exactly equal to two during transients or during steady-state if the DC gain of the plant model is inaccurate. One way to alleviate these issues is to introduce a feedback structure.

In the sFF + PI control configuration, a static feedforward compensator calculates the optimal oxygen excess ratio at steady-state, given a measurement of the stack current I_{st}. Then the PI controller adjusts the compressor motor voltage v_{cm} to regulate λ_{O2} about the optimal value calculated by the feedforward block in Fig. 5(b). Unlike sFF, the static map $g_{sff+PI}(I_{st})$ is a lookup table that determines the optimal λ_{O2} for a given I_{st}. We construct this lookup table by first simulating the model at various I_{st} and v_{cm} values and then plotting the corresponding steady-state values of net power P_{net} and λ_{O2}, shown in Fig. 6(a). Next we identified the value of λ_{O2} that maximizes P_{net} given I_{st}, which produced the lookup table shown in Fig. 6(b). In contrast to sFF, this approach determines the optimal set point for λ_{O2} related to the disturbance I_{st}. However, it has two distinct drawbacks. First, the optimal λ_{O2} value identified by the lookup table corresponds to steady-state response values only. As a result, optimality is not guaranteed during transients. Second, the lookup table is generated for a fuel cell stack temperature of T_{fc} = 353 K and membrane water content of λ_m = 14. As demonstrated in Section III, the optimum λ_{O2} is quite sensitive to these system parameters. Hence, optimality is only guaranteed when these conditions are met exactly.

B. Performance

To illustrate how ES optimizes net power, we simulate the responses of compressor motor voltage v_{cm}, oxygen excess ratio λ_{O2}, and net power P_{net} to a stack current I_{st} input of 150A for the sFF, sFF + PI, and ES control architectures. The initial conditions are set to correspond with the steady-state values produced for operating conditions of T_{fc} = 353K and λ_m = 14. However, in these simulations we set T_{fc} = 293K and λ_m = 6 to understand how each controller deals with varying operating conditions. Similar results may be obtained with step or ramp inputs; however, a constant input and the aforementioned initial conditions provide results that are sufficient for understanding the fundamental performance differences among the control architectures. The perturbation frequency ω is set to 0.15 rad/sec. The band-pass filter is a third order Butterworth filter with cut-off frequencies at 0.07 and 0.3 rad/sec.

In Fig. 7, we observe that ES generates final values of P_{net} = 22.5 kW and λ_{O2} = 2.64 that correspond to the optimal values found by the steady-state analysis in Fig. 3. The corresponding optimal compressor motor voltage is 151V. Moreover, the net

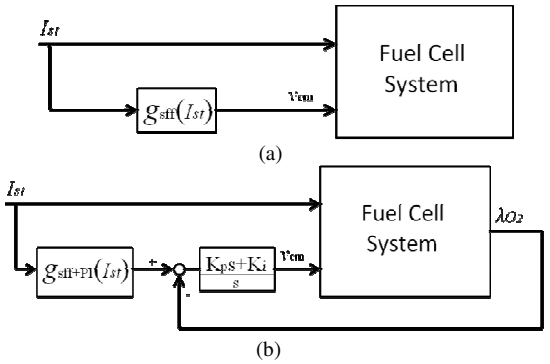

Fig. 5(a) Static feedforward (sFF) and (b) Static feedforward with PI control (sFF + PI) architectures.

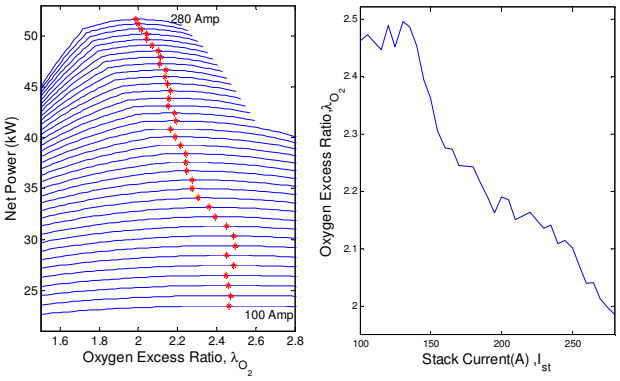

Fig. 6(a) Net power at different stack current from $g_{sff+PI}(I_{st})$, (b) Look-up table for $g_{sff+PI}(I_{st})$

power values generated are higher than either sFF or sFF + PI at steady-state. This indicates that the ES algorithm effectively identifies the optimal net power and oxygen excess ratio despite variations in stack temperature and membrane water content and produces superior power output relative to both sFF and sFF + PI.

Typically, if one wishes to enforce the set constraints (23) and (24) without penalty functions, the ES parameters a, k, ω must be chosen conservatively and slowly increased until satisfactory results are obtained. However, the approach proposed here explicitly accounts for these constraints through a penalty function transformation. Therefore, there exists more freedom in selecting aggressive ES parameters. This is advantageous because the constrained ES algorithm guarantees that set constraints (23) and (24) are enforced and allows greater values of a and k, which increases the convergence speed [14], [16], but may result in overshoot. In Fig. 8, we investigate this property by running simulations for various values of k. These results show the net power output reaches the optimal value more quickly as k increases. However, it also makes the compressor motor voltage input more sensitive to perturbations, resulting in greater overshoot. Hence, applying penalty functions enables more aggressive ES parameter choices, which increases convergence speed with higher overshoot. Nevertheless, the penalty functions mitigate the tradeoff imposed by Assumption 3 of Section IV

to an extent, and allow faster convergence speed within an acceptable overshoot range.

C. Discussion

These simulation results indicate that ES converges to the optimal operating point and can account for time-varying parameters, such as stack temperature and membrane water content, by searching for the optimal compressor motor voltage online. The constrained extremum seeking approach allows the engineer to explicitly enforce set constraints representing sufficient membrane hydration and reactant oxygen supply. An additional benefit of the penalty functions is that it enables the designer to select more aggressive ES parameters to increase convergence speed, with satisfactory overshoot.

Despite ES's many desirable properties, it also comes with several drawbacks. First, the periodic perturbation may produce unacceptable oscillations in the system. Secondly, the ES algorithm presented here generally takes a long time to converge, even with penalty functions that allow for more aggressive ES parameters. This is a direct result of requiring the perturbation frequency to be at least one order of magnitude less the plant's slowest eigenvalue. Third, when the system reaches the optimal operating point, the system oscillates about this value rather than converging to it exactly. In future work, we shall apply two techniques to resolve these drawbacks. First, we will investigate alternative periodic signal designs (e.g. square and saw-tooth waves) to determine if they improve convergence speed, as suggested by [22]. Second, we will apply a periodic perturbation signal with dynamic amplitude that converges to zero as ES converges to the optimal value u^*. One simple method for doing this is to make the periodic perturbation signal exponentially decaying in amplitude [21].

VI. Conclusion

This paper investigates a novel constrained extremum seeking method for maximizing the net power output of a PEM fuel cell system. First we review a popular model in the literature [6], [7] and analyze how the net power production changes with varying stack temperature and membrane water content. Then we define an optimal control problem with set constraints defining admissible state and control values. Finally, we simulate the proposed ES algorithm and compare its results against simple open loop and closed loop control architectures. The results indicate that ES is able to improve the net power output relative to the other controllers, despite variations in stack temperature and membrane water content. Moreover, exterior point penalty functions effectively enforce the set constraints and enable the use of more aggressive ES parameters to increase convergence speed for an appropriate level of overshoot.

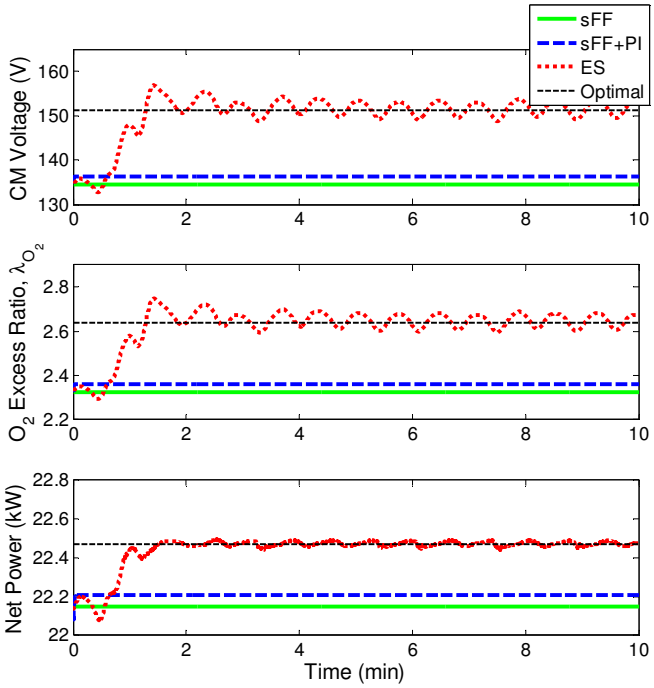

Fig. 7. Comparison of simulation results for each control architecture with initial conditions T_{fc} = 353K and λ_m = 14 simulated at T_{fc} = 293K and λ_m = 6 , with ES parameters a = 2 and k = 12.

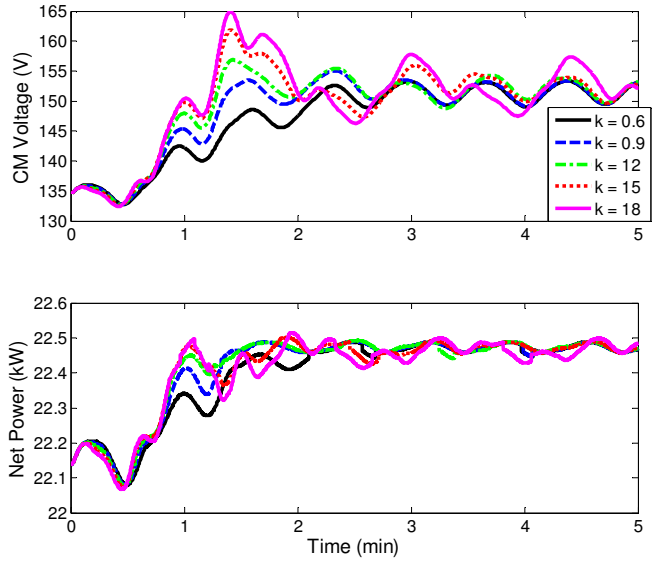

Fig. 8. Net power response for various values of ES parameters k. Note the tradeoff between convergence speed and overshoot.

Acknowledgment

The authors thank Professor Anna Stefanopoulou at the University of Michigan, Ann Arbor for her advice, helpful discussions, and Fall 2007 ME569 class "Control for Advanced Powertrain Systems," which served as the inspiration for this paper.

REFERENCES

[1] J. M. Cunningham, D.J. Friedman, M.A. Hoffman, R.M. Moore, "Requirements for a flexible and realistic air supply model for incorporation into a fuel cell vehicle (FCV) system simulation", *SAE Paper 1999-01-2912* in SP-1466, 1999, pp. 43-48.

[2] J. T. Pukrushpan, A. G. Stefanopoulou and H. Peng, "Modeling and control for PEM fuel cell stack system," in *Proceedings of 2002 American Control Conference,* 2002, pp. 3117-3122.

[3] R. T. Meyer and S. Revankar, "A survey of PEM fuel cell system control models and control developments," in *4th International ASME Conference on Fuel Cell Science,Engineering and Technology, FUELCELL2006,* 2006, pp. 17.

[4] Y. Yang, F. Wang, H. Chang, Y. Ma and B. Weng, "Low power proton exchange membrane fuel cell system identification and adaptive control," *Journal of Power Sources,* vol. 164, pp. 761-771, 2007.

[5] J. Golbert and D. R. Lewin, "Model-based control of fuel cells: (1) regulatory control," *Journal of Power Sources,* vol. 135, pp. 135-51, 2004.

[6] J. T. Pukrushpan, H. Peng and A. G. Stefanopoulou, "Control-oriented modeling and analysis for automotive fuel cell systems," *Journal of Dynamic Systems, Measurement and Control, Transactions of the ASME,* vol. 126, pp. 14-25, 2004.

[7] J. T. Pukrushpan, "Modeling and Control of Fuel Cell Systems and Fuel Processors," Ph.D. dissertation, Dept. of Mech. Eng., University of Michigan, Ann Arbor, MI, 2003.

[8] B. A. McCain, A. G. Stefanopoulou and I. V. Kolmanovsky, "A multi-component spatially-distributed model of two-phase flow for estimation and control of fuel cell water dynamics," *2007 46th IEEE Conference on Decision and Control,* pp. 584-589, 2007.

[9] B. A. McCain, A. G. Stefanopoulou and I. V. Kolmanovsky, "On the dynamics and control of through-plane water distributions in PEM fuel cells," *Chemical Engineering Science,* vol. 63, pp. 4418-4432, 2008.

[10] Z. Zhong, H. Huo, X. Zhu, G. Cao and Y. Ren, "Adaptive maximum power point tracking control of fuel cell power plants," *Journal of Power Sources,* vol. 176, pp. 259-269, 2008.

[11] J. Zhang, G. Liu, W. Yu and M. Ouyang, "Adaptive control of the airflow of a PEM fuel cell system," *Journal of Power Sources,* vol. 179, pp. 649-59, 05/01. 2008.

[12] Y. F. Xiong, "Modeling and Control of a Small PEM Fuel Cell Flow System," Ph.D. dissertation, Institute of Automation, Chinese Academy of Sciences, 2006.

[13] K. B. Ariyur, M. Krstić, *Real-Time Optimization by Extremum Seeking Control*, Hoboken, NJ: Wiley, 2003.

[14] M. Krstić and H.-H. Wang, "Stability of extremum seeking feedback for general nonlinear dynamic systems," *Automatica,* vol. 36, pp. 595-601, 04. 2000.

[15] N. J. Killingsworth and M. Krstić, "PID tuning using extremum seeking: online, model-free performance optimization," *IEEE Control Systems Magazine,* vol. 26, pp. 70-79, 2006.

[16] Y. Tan, D. Nesic and I. Mareels, "On non-local stability properties of extremum seeking control," *Automatica,* vol. 42, pp. 889-903, 06. 2006.

[17] K. S. Peterson and A. G. Stefanopoulou, "Extremum seeking control for soft landing of an electromechanical valve actuator," *Automatica,* vol. 40, pp. 1063-1069, 2004.

[18] M. Guay, N. Peters and D. DeHaan, "Real-time dynamic optimization of batch systems," *Journal of Process Control,* vol. 17, pp. 261-71, 03. 2007.

[19] C. Zhang and R. Ordonez, "Numerical optimization-based extremum seeking control with application to ABS design," *IEEE Transactions on Automatic Control,* vol. 52, pp. 454-67, 03. 2007.

[20] P. Y. Papalambros, D. J. Wilde, *Principles of Optimal Design: Modeling and Computation* 2nd ed., New York, NY: Cambridge University Press, 2000, ch. 7.

[21] D. DeHaan and M. Guay, "Extremum-seeking control of state-constrained nonlinear systems," *Automatica,* vol. 41, pp. 1567-1574, 2005.

[22] Y. Tan, D. Nesic and I. Mareels, "On the choice of dither in extremum seeking systems: A case study," *Automatica,* vol. 44, pp. 1446-1450, 2008.